3984–3998 *Nucleic Acids Research, 2010, Vol. 38, No. 12* *Published online 9 March 2010*
doi:10.1093/nar/gkq144

Telomeric protein TRF2 protects Holliday junctions with telomeric arms from displacement by the Werner syndrome helicase

Gerald J. Nora[1], Noah A. Buncher[1] and Patricia L. Opresko[1,*]

[1]Department of Environmental and Occupational Health, University of Pittsburgh Graduate School of Public Health, Pittsburgh, PA 15219, USA

Received January 8, 2010; Revised February 13, 2010; Accepted February 18, 2010

ABSTRACT

WRN protein loss causes Werner syndrome (WS), which is characterized by premature aging as well as genomic and telomeric instability. WRN prevents telomere loss, but the telomeric protein complex must regulate WRN activities to prevent aberrant telomere processing. Telomere-binding TRF2 protein inhibits telomere t-loop deletion by blocking Holliday junction (HJ) resolvase cleavage activity, but whether TRF2 also modulates HJ displacement at t-loops is unknown. In this study, we used multiplex fluorophore imaging to track the fate of individual strands of HJ substrates. We report the novel finding that TRF2 inhibits WRN helicase strand displacement of HJs with telomeric repeats in duplex arms, but unwinding of HJs with a telomeric center or lacking telomeric sequence is unaffected. These data, together with results using TRF2 fragments and TRF2 HJ binding assays, indicate that both the TRF2 B- and Myb domains are required to inhibit WRN HJ activity. We propose a novel model whereby simultaneous binding of the TRF2 B-domain to the HJ core and the Myb domain to telomeric arms promote and stabilize HJs in a stacked arm conformation that is unfavorable for unwinding. Our biochemical study provides a mechanistic basis for the cellular findings that TRF2 regulates WRN activity at telomeres.

INTRODUCTION

Lack of the Werner protein (WRN) causes Werner syndrome (WS), a segmental progeroid disorder characterized by cellular genomic and telomeric instability and premature senescence (1,2). WRN is a RecQ family helicase that is unique among the five human RecQ helicases for also having an exonuclease domain (3). Many of the RecQ helicases, in general, are thought to function during DNA replication to prevent replication fork demise and to restore stalled or broken replication forks, partly through homologous recombination (HR) pathways (4). Consistent with this, WRN protein is implicated in pathways for recombinational repair of stalled replication forks and DNA double-strand breaks (5,6). WRN is proposed to have particularly important roles in telomere preservation during replication. Telomeres protect chromosomes ends, and telomere dysfunction triggers cellular senescence, apoptosis or genomic instability (7). The forced expression of telomerase in WS fibroblasts suppresses many of the primary cellular defects, including telomere loss on sister chromatids (8), premature senescence (9) and the accumulation of chromosomal aberrations (10). Cellular and biochemical data indicate that WRN may preserve telomeres by dissociating alternate DNA structures to facilitate replication fork progression or for completion of HR repair at stalled or broken replication forks (2). These DNA structures include G-quadruplexes, four-way junctions that mimic regressed replication forks and Holliday Junction (HJ) intermediates in HR, and D-loop structures that occur during HR and at the telomeric end (11,12). All of these are preferred substrates for WRN helicase which can also branch migrate HJ and D-loops (12,13). These studies suggest that inappropriate processing of alternate structures at telomeres can lead to premature telomere loss and cell senescence or apoptosis.

Human telomeres are characterized by repetitions of a short sequence of duplex DNA (TTAGGG) and a 3′ overhang of single-stranded DNA (ssDNA), bound by the shelterin complex of six proteins (7,14). The 3′ overhang, which may be 50–500 nt, is bent around into a t-loop and then invades the duplex DNA, displacing

*To whom correspondence should be addressed. Tel: +1 412 624 8285; Fax: +1 412 624 9364; Email: plo4@pitt.edu

the G-rich strand and forming a displacement loop (D-loop) (15). Telomere D-loop formation is thought to be mechanistically similar to D-loop formation during the initiation of HR (7,16,17). The shelterin protein TRF2 is critically important for stimulating formation and preservation of the telomeric t-loop/D-loop structure (18–20). TRF2 has two DNA-binding domains: an N-terminal basic domain that binds four-way junctions regardless of sequence (21) and a C-terminal Myb domain that specifically binds duplex TTAGGG repeats (22). Cellular studies showed that the overexpression of TRF2 lacking the B-domain (TRF2ΔB) results in cleavage of the t-loop/D-loop by HJ resolvase XRCC3 (16), which leads to extra-chromosomal telomeric circles that can be visualized by two-dimensional (2-D) electrophoresis and electron microscopy (16,23). TRF2 binds to and inhibits cleavage of four-way junction models of HJ structures *in vitro* (21,24). WRN is required for the production of telomeric circles in TRF2ΔB overexpressed cells (25), but the mechanism is unknown. Interestingly, in telomerase-positive WS cells, telomeric circles form in the absence of WRN and independently of XRCC3, implicating WRN in more than one pathway for telomere stability (25). While TRF2 is known to protect HJs from cleavage by HJ resolvases (24), whether TRF2 also regulates displacement and migration at the telomere t-loop/D-loop is not known.

One model for WRN promotion of telomeric circles in TRF2ΔB expressing cells is that WRN stimulates branch migration of the t-loop/D-loop into a target for cleavage. HJ-like structures also form preferentially at telomeres during replication fork regression that produces a four-way junction in which one duplex end is accessible (chicken foot) (26). WRN exonuclease can attack this vulnerable end, and the helicase can displace the four-way junction (27). Both TRF2 and WRN bind the HJ core *in vitro* (21,28). Therefore, it is possible that TRF2 may protect HJs from WRN activity by inhibiting WRN loading. Paradoxically, TRF2 binds directly to WRN protein *in vivo* (25,29,30), and *in vitro* studies showed that TRF2 recruits WRN to telomeric substrates (29), stimulates WRN exonuclease digestion of telomeric duplexes (29) and stimulates WRN helicase unwinding of short forks (30). Whether TRF2 modulates WRN processing of HJ DNA is not known.

Given that TRF2 represses WRN promotion of t-circles (25), in this study, we tested the hypothesis that TRF2 negatively regulates WRN activity on four-way structures that may occur at the t-loop/D-loop or during replication fork regression. By testing a variety of HJ substrates containing site-specific blocks to WRN helicase 3′–5′ translocation, we provide evidence that WRN displaces four-way structures from the center moving outward. We also found that TRF2 protects telomeric HJ DNA against WRN strand displacement activity. However, both the TRF2 B and Myb DNA-binding domains are required for WRN inhibition, indicating that TRF2 must engage both the HJ core and the duplex arms to regulate WRN strand displacement.

MATERIALS AND METHODS

Proteins

Recombinant human hexahistidine-tagged WRN protein and the exonuclease-dead E84A WRN mutant (X-WRN) were purified from a baculovirus/insect cell expression system as described previously (31). Recombinant human hexahistidine-tagged RPA was provided as a gift from Dr Walter Chazin (Vanderbilt University, TN, USA). Recombinant human hexahistine-tagged TRF2 protein was purified as formerly described (30). Recombinant hexahistine TRF2 protein fragment (amino acids 45–501; TRF2ΔB) was generated by polymerase chain reaction (PCR) cloning using the TRF2 cDNA from the baculovirus DNA construct, kindly provided by Dr Titia de Lange (Rockefeller University, New York, NY) as a template. The PCR product was subcloned into the BamHI and EcoRI sites of the pRSET-A expression vector (Invitrogen, Carlsbad, CA). The TRF2ΔB fragment was expressed in BL21(DE3) *Escherichia coli* and purified with an AKTA Explorer FPLC (GE Life Sciences, Piscataway, NJ). After the induction of TRF2ΔB expression with 1 mM isopropyl-β-D-thiogalactoside (IPTG) for 4 h at 30°C, cells were harvested and resuspended in lysis buffer (20 mM NaH_2PO_4, 0.5 M NaCl, 10 mM imidazole, 1% NP-40 and 5 mM beta-mercaptoethanol) and mixed on a rotator at 4°C for 30 min. Protease inhibitors were included in all buffers (Roche Molecular Biochemicals, Indianapolis, IN). Cells were centrifuged at 15 000r.p.m. for 30 min at 4°C. The supernatant was loaded onto a HisTrap FF (GE Life Sciences) column equilibrated with lysis buffer. The column was washed with buffer A (20 mM NaH_2PO_4, 0.5 M NaCl) containing 10 mM imidazole, and subsequently washed and protein eluted with 60 mM and 100 mM imidazole, respectively. The eluant was dialyzed against buffer D (20 mM HEPES, pH 7.9, 100 mM KCl, 3 mM $MgCl_2$, 1 mM DTT, 20% glycerol, 0.5 mM PMSF) in Slide-a-lyzer cassettes (Thermo Fisher, Rockford, IL, USA) at 4°C. Protein purity and concentration were determined by SDS PAGE Coomassie analysis and Bradford assay, respectively. The pGEX4T-RAP1 construct was kindly provided by Dr Zhou Songyang (Baylor College of Medicine, Houston, TX). GST-tagged human RAP1 was expressed in BL21 (DE3) *E. coli* and purified on glutathione Sepharose beads (GE Life Sciences) in batch followed by Thrombin (GE Healthcare) cleavage as previously described with some modification (32). Following the induction of RAP1 expression with 1 mM IPTG for 2 h at 37°C, cells were harvested at 3800 r.p.m. for 15 min at 4°C, resuspended in lysis buffer (1X PBS, protease inhibitors, 50 mM beta-mercaptoethanol and 1% Triton X-100), sonicated and mixed in a rotator for 15 min at 4°C. Cell lysate was harvested at 10 000 r.p.m. for 10 min, and the supernatant was incubated with glutathione-Sepharose beads (GE Healthcare, Piscataway, NJ) for 3 h at 4°C on a rotator. Bound GST-tagged RAP1 was cleaved with Thrombin (GE Healthcare) for 12 h at 4°C. The supernatant was loaded onto a Mono Q 5/50 GL (GE Life Sciences) column

equilibrated with buffer A (150 mM Tris, pH 8.0, 50 mM NaCl, 0.05% NP-40 and 10% glycerol). RAP1 protein was eluted in buffer B (150 mM Tris pH 8.0, 10% glycerol and 0.05% NP-40) at 335 mM NaCl. Protein purity and concentration were determined by sodium dodecyl sulfate polyacrylamide gel electrophoresis, (SDS–PAGE) Coomassie analysis and Bradford assay, respectively.

DNA substrates

All oligonucleotides were purchased from Integrated DNA Technologies (Coralville, IA, USA) and PAGE-purified by the manufacturer, except for HJbio-4, which was purchased from and PAGE-purified by Gene Link (Hawthorn, NY, USA). Fluorescent labels were covalently linked to the 5′ nucleotide by the manufacturer. Sequences are provided in Supplementary Table S1.

All HJ constructs, modified from the XJ12 described previously (11) and with the exception of HJT (Table 1), were annealed in 25 µl reaction volumes. For HJ DNA constructs, 10 or 12 pmol of the indicated oligonucleotide 1 was mixed with a 1:2:3:2 molar ratio with the respective 2, 3 and 4 oligonucleotides (Table 1), respectively, in 0.35× PBS and 350 mM LiCl. The oligonucleotides were annealed in a TC-312 PCR machine (Techne, Burlington NJ) by incubating at 95°C for 5 min, followed by cooling to 65°C at 1°/min.The reactions were held at 65°C for 5 min, cooled to 37°C at 1°/min, then incubated at 37°C for 8 h and then cooled to 10°C.

The HJT construct was prepared by first annealing the forked halves of the substrate separately in 12.5 µl reactions with 100 mM LiCl and 0.5× TE buffer: one with 10 pmol T-1 and 20 pmol T-2, and the other with 40 pmol T-3 and 20 pmol T-4. The reactions were incubated at 65°C for 5 min and allowed to cool to 37°C. To form HJT the separate forked duplex reactions were combined, incubated at 37°C for 1 h and cooled to room temperature.

A portion of each HJ preparation (0.5 µl) was removed for use as a standard to determine the concentration of the purified HJ preparations. The remainder was mixed with 16 µl H_2O and 7.5 µl 80% glycerol and loaded on an 8% polyacrylamide gel. Voltage (150 V) was applied for 1.5 h at 4°C. The HJ products were visualized by fluorescence on a Typhoon Imager (GE Healthcare), excised from the gel and purified from the gel slice by electroelution for two hours in a Model 422 Electroeluter (Bio-Rad, Hercules CA). The eluant was concentrated in a Microcon YM-30 (Millipore, Billerica MA) and resuspended in 100 µl of storage buffer (10 mM Tris pH 7.5, 10 mM $MgCl_2$) and stored at –20°C. Purification quality and yields were determined by analysis on 8% native polyacrylamide gels, followed by visualization and quantitation with a Typhoon Imager and ImageQuant software (GE Healthcare, Piscataway, NJ, USA).

Forked duplexes were prepared by annealing oligonucleotides as described in Supplementary Table S1 in 1:1 molar ratios. Annealing reactions (50 µl) were incubated in 50 mM $LiCl_2$ and 0.71× PBS at 95°C for 5 min and then allowed to cool to room temperature.

Table 1. Holiday junction substrates used in this study

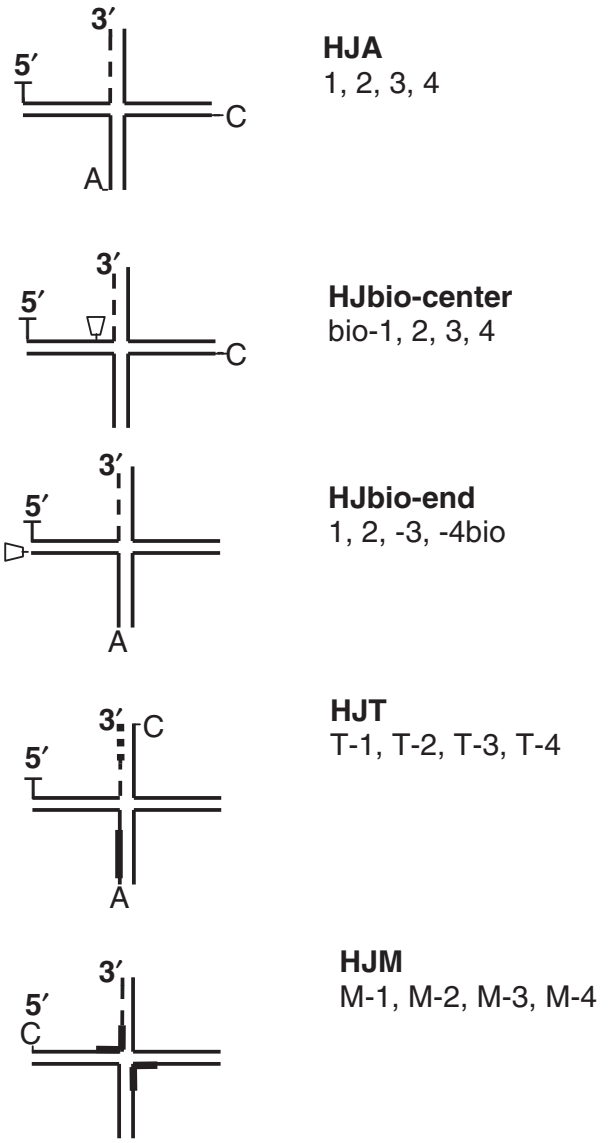

T = TAMRA; C = Cy5; A = Alexa488. Dotted lines denote an oligonucleotide with an exonuclease-vulnerable 3′-end lacking a thiophosphate bond protection. Bolded lines indicate the G-rich strand of telomeric repeats. Numbers under the name of the construct denote the oligonucleotides used to create the construct (see Supplementaary Table S1),

Helicase/exonuclease reactions

HJ substrates were reacted in standard reaction buffer (40 mM Tris pH 7.5, 4 mM $MgCl_2$, 5 mM DTT, 0.1 mg/ml BSA and 2 mM ATP) at 37°C for various time points as indicated in the figure legends. The concentrations of substrate and proteins WRN, X-WRN, TRF2, TRF2ΔB and RPA were as indicated in the figure legends. Reactions were started by WRN or X-WRN addition, and terminated by adding 2.7X stop dye [50 mM ethylenediaminetetraacetic acid (EDTA), 40% glycerol]. The reactions that included RPA and/or TRF2 were

terminated with 2.7X ProtK-SDS stop dye (15 mM EDTA, 1 μg/ml proteinase K, 300 mM LiCl, 1.5% SDS) and incubated at 37°C for 30 min. As SDS fluoresces and interferes with analysis of the fluorescent substrates, it was precipitated based on a protocol by Zhitkovich and Costa (33). Briefly, 4 μl 1 M KCl was added to the 31.5-μl stopped reactions, followed by incubation on ice for 5 min. The precipitate was pelleted by centrifugation for 10 min at 10 000*g* at 4°C. The supernatant (31 μl) was drawn off and transferred to a fresh tube with 15 μl of loading buffer (40% glycerol, 0.5× TE). The SDS precipitation procedure did not result in any significant reannealing of the dissociated ssDNA products (Supplementary Figure S1). The terminated reactions were run on either 8% or 12% native polyacrylamide gels as indicated in the figure legends at 150 V.

The TAMRA, Cy5 and Alexa488 fluorophores were visualized on a Typhoon Imager using the preset TAMRA, Cy5 and Alexa488 laser excitation and emission settings, with a photomultiplier gain of 575 V for all channels and normal sensitivity. Control reactions ensured that cross-talk between channels did not occur (data not shown). Reaction substrates and products were quantified using ImageQuant 5.1 (GE Life Sciences) software. The local median analysis was used for background correction. Substrate and products were calculated as the percent of the total DNA in each lane for each fluorophore. All values were corrected for background in the no protein and boiled control lanes as described previously (34).

Electrophoretic mobility shift assay

Binding reactions (10 μl) contained standard reaction buffer (40 mM Tris pH 7.5, 4 mM $MgCl_2$, 5 mM DTT, 0.1 mg/ml BSA, 2 mM ATP), 5% glycerol and 5 nM DNA substrate. The reactions were initiated by adding various concentrations of TRF2, as indicated in the figure legend, and were incubated for 20 min at room temperature. The reactions were loaded on 1% agarose gels and electrophoresed in 0.5× TBE at 4°C and 140 V for 1 h. The fluorescent products and substrates were visualized and analyzed as described for the helicase reactions.

RESULTS

WRN helicase and exonuclease activities simultaneously process HJs

Prior to investigating TRF2 modulation of WRN activity on HJ substrates, we required a more complete understanding of WRN mechanism for HJ dissociation. Previous independent studies demonstrated WRN exonuclease activity at the 3′ blunt end of a static four-way junction (27) and WRN helicase dissociation of a four-way junction with a mobile homologous core (11). Therefore, we asked whether both activities could simultaneously process a model HJ with a mobile core. To test this, we developed a multiplex fluorophore imaging method to track the fate of individual strands of a four-way construct in which three strands were labeled with a unique fluorophore. Previous studies with four-way junctions monitored substrate conversion to ssDNA by tracking migration of one radiolabeled strand in the construct. While current fluorophores still suffer the disadvantage of decreased sensitivity compared to ^{32}P radioactivity, they offer the distinct advantage of identifying the exact oligonucleotide composition of all intermediates and products present in each band on a gel. This is particularly critical if the HJ construct is asymmetric due to the presence of telomeric repeats or chemically modified bases in some arms, as in many of the HJs in this study (Table 1).

Each arm of the HJA construct (Table 1) is 25 bp long with a 12-nt homologous center (11). Since a four-way junction is unlikely to have four exposed ends *in vivo*, all the 3′ ends except for the T-oligonucleotide contained a thiophosphate bond to protect against exonuclease activity. One exposed end mimics a regressed replication fork which is thought to be a target for WRN (5,28,35). WRN processing of the HJA substrate led to a variety of displaced DNA products that were uniquely identified by their fluorescent tags (potential products shown separately in Supplementary Figure S2). The appearance of a forked duplex preceded the appearance of ssDNA product (Figure 1A), as shown schematically in Figure 1B. The distribution of the T-oligo, which contains the unprotected 3′end, among the various intermediates and products was quantitated (Figure 1C). In the first 8 min of the reaction <5% of the HJ was unwound and the predominant displaced T-oligo species was an intact fork duplex (3% of the total DNA) [Figure 1A (lanes 2–10) and C]. After 16 min, both T-oligo exonuclease degraded fork (exo-fork) and ssDNA (exo-ssDNA) species began to predominate (8% and 3%, respectively), and increased linearly with time to 19% and 18%, respectively, at 60 min (Figure 1C). After 60 min the amount of intact T-oligo in a fork or as ssDNA was low (<3%) or negligible, respectively, indicating robust WRN exonuclease attack of the vulnerable arm during the reaction (Figure 1D). Upon completion the A-oligo, which pairs with both the T- and C-oligos in the HJ, was evenly divided between an intact fork with the C-oligo (8%) and a degraded fork with the T-oligo (11%; Figure 1D). Similar amounts of fork and ssDNA product were detected for each oligo, indicating no apparent bias for dissociation of any of the arms (Figure 1D). Our data are consistent with a mechanism for HJ processing in which WRN simultaneously displaces the HJ into forks while degrading the vulnerable T-oligo, followed by fork displacement to ssDNA.

WRN helicase initiates HJ strand displacement at the center and translocates outward

WRN binds the HJ core and is presumed to initiate unwinding from the center (28). However, while WRN helicase is inactive on blunt ended dsDNA, the WRN exonuclease can digest the blunt ends of substrates that contain junctions such as forks, bubbles or HJs,

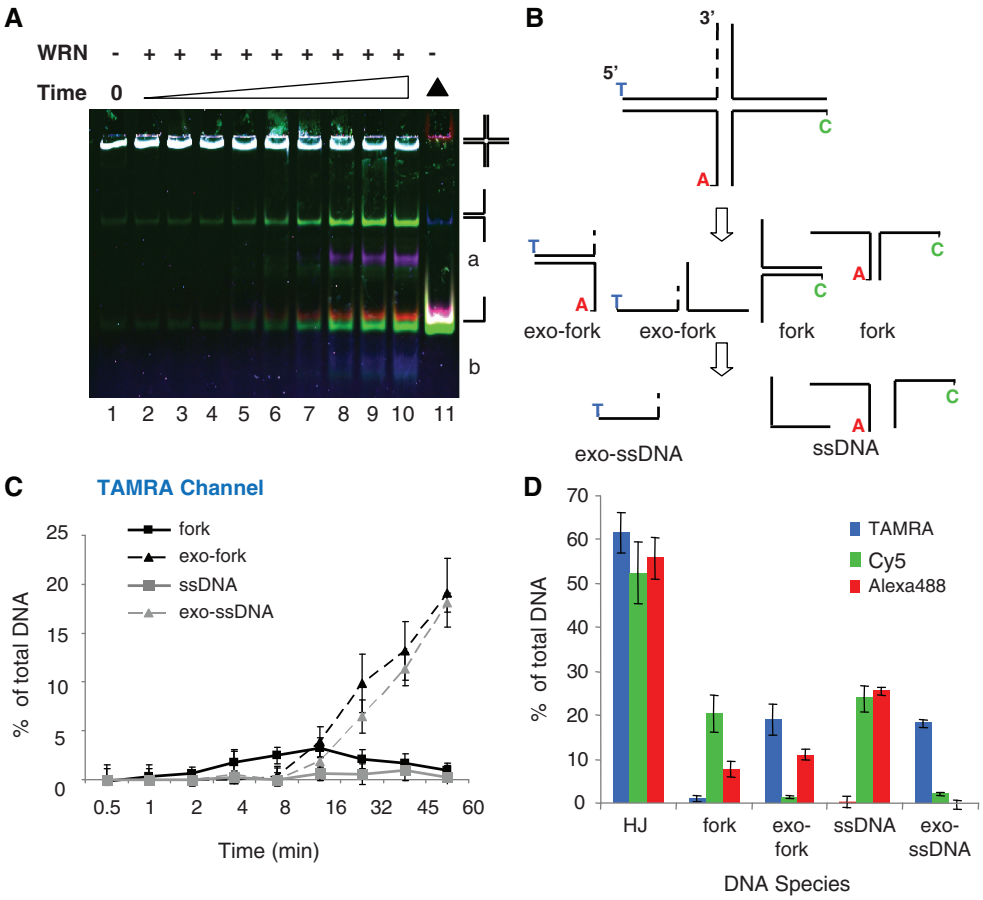

Figure 1. WRN helicase and exonuclease simultaneously process HJ substrates with a mobile core. (**A**) HJA (2 nM) was incubated with 24 nM WRN in standard reaction buffer at 37°C. Aliquots were terminated at various times from 0.5 to 60 min in 2-fold increments (lanes 2–10). Reactions were run on a 12% native polyacrylamide gel and were visualized with a Typhoon Imager in the TAMRA (blue), Cy5 (green) and Alexa 488 (red) channels. Colors assigned by Imagequant software. The exonuclease degraded products are indicated as (a) = exo-fork and (b) = exo-ssDNA. (**B**) Schematic of WRN strand displacement and exonuclease products. T = TAMRA, C = Cy5 and A = Alexa488 labeled oligonucleotides. The 3′ end of the exonuclease vulnerable T-oligo is highlight as a dotted line. (**C**) The percent of displaced T-oligo products from the reactions in (**A**) were quantitated as described in 'Materials and Methods' section and plotted against time. Intact fork, solid black line and squares; exonuclease-degraded fork, dashed black line and triangles; intact ssDNA, solid gray line and squares; exonuclease-degraded ssDNA, dashed gray line and triangles. (**D**) Substrate and product distribution for each labeled oligonucleotide in the HJ construct after 1 h reaction. The percent of T-, A- and C-oligos present in the HJ substrate and each intermediate and product were quantitated as a function of total oligonucleotide as described in 'Materials and Methods'. Values represent the mean and standard deviation of two or three separate experiments.

presumably by WRN first loading at the junction site (28). Therefore, it is formally possible that WRN helicase may also initiate strand displacement from the blunt end of an HJ, such as at a regressed replication fork, which may bypass effects of TRF2 bound at the core. To test the mechanism of HJ unwinding we used strategically placed biotin/streptavidin blocks. We and others showed that while a biotin does not interfere with WRN helicase activity (Supplementary Figure S1), a biotin/streptavidin complex can inhibit strand displacement (12). Control experiments confirmed that a biotin/streptavidin complex inhibits X-WRN unwinding of a forked duplex only when present on the translocating strand (Figure 2A), but not when present on the non-translocating strand (Figure 2B). Slower migration of the fork and ssDNA product upon streptavidin addition confirms the presence of a biotin/streptavidin complex. An exonuclease-dead variant of WRN (X-WRN) was used to examine helicase alone. Since WRN helicase is poorly processive, RPA was required to increase product yield for detection of potential inhibition, but did not relieve the biotin/streptavidin block to WRN unwinding and does not melt the duplex (Supplementary Figure S3).

We reasoned that if WRN initiates unwinding from the HJ center then a biotin/streptavidin block at the core, 24 nt from the 5′-end of the T-oligo (HJbio-center), would inhibit WRN 3′–5′ translocation on the T-oligo through the T/A duplex arm (Figure 3A III, open arrows). However, unwinding in the 'vertical' axis (dark arrows) would be permitted (Figure 3A, dark arrows) yielding products that included the T-oligo trapped in a fork with the A-oligo. When HJbio-center was incubated with X-WRN and RPA, 47% and 89% of the T- and A-oligos were liberated as ssDNA, respectively [Figure 3B and C (lane 2), and 3D]. Some of the T-oligo

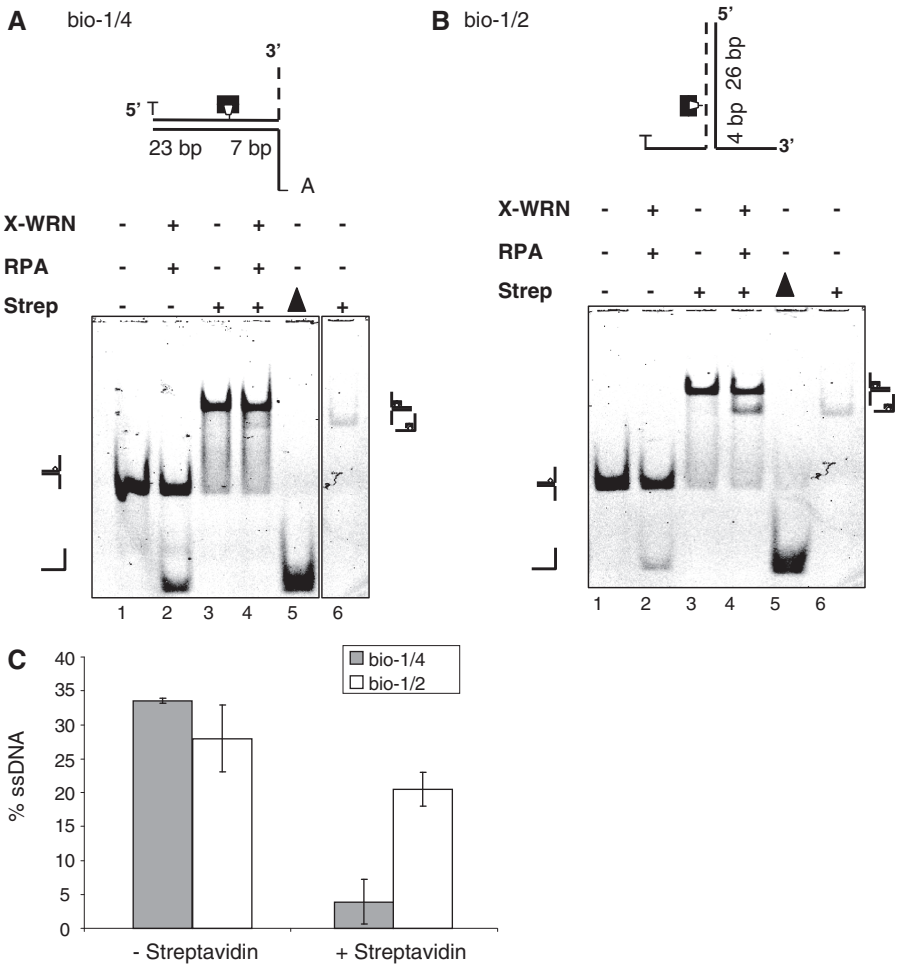

Figure 2. A biotin–streptavidin complex on the translocating strand of a forked duplex inhibits WRN unwinding activity. Reactions contained a 31-bp forked duplex (0.5 nM) with a biotinylated nucleotide (inverted trapezoid) on the WRN translocating (**A**) or nontranslocating strand (**B**). Black box denotes streptavidin. The forks were constructed by annealing oligonucleotides bio-1 and 4 (A) or bio-1 and 2 (B) (Supplementary Table S1). T = TAMRA; A = Alexa488. The duplex length (bp) on either side of the biotinylated nucleotide is shown. The substrate was pre-incubated with either 0 (lanes 1 and 2) or 30 nM (lanes 3 and 4) streptavidin in standard reaction buffer prior to adding 3.4 nM X-WRN and 12 nM RPA. Reactions were for 20 min at 37°C, and were run on an 8% native polyacrylamide gel for 2.5 h and visualized with a Typhoon imager. A streptavidin-bound T-oligo was loaded (lane 6) as a marker and the boiled substrate lane is indicated with a triangle (lane 5). The gel scans show the TAMRA emission channel. (**C**) Quantitation of the ssDNA product. The percent of ssDNA T-oligo product was quantitated as described in 'Materials and Methods' section. Values represent the mean and SEM. from two independent experiments.

was released as a fork with the unlabeled oligo, but not with the A-oligo, perhaps due to greater G/C content on the HJ arm composed of the T-oligo and the unlabeled strand (Supplementary Table S1). Upon streptavidin addition, the displaced ssDNA product decreased substantially to 17% and 55% for the T- and A-oligos, respectively [Figure 3B and 3C (lane 5), and 3D]. Importantly, streptavidin addition yielded a novel forked species consisting of the T- and A-oligos (total of 31% and 15%, respectively, since a T/unlabeled fork is also present) and a novel triple stranded species consisting of the T- and A-oligos (17% and 15%, respectively) bound to the unlabeled oligo. These species contained negligible amounts of C-oligo (1%) (data not shown) and the three-way probably resulted from shifting between two conformations (Figure 3E). The 12-nt homologous core can shift the biotin/streptavidin block from the T/A duplex arm (Figure 3A, I and II) to the T/unlabeled duplex arm (Figure 3A, III), whereas the C-oligo is never present in a duplex arm with a biotin (Figure 3A). These dynamic conformations likely explain the lack of complete WRN inhibition and the generation of a novel three-way species by a biotin/streptavidin barrier at the HJ core.

To test whether WRN can load on the HJ blunt end and translocate toward the center while unwinding, we asked if a 3′ biotin/streptavidin complex on the A-oligo would inhibit WRN helicase activity (HJbio-end) (Figure 4A). In contrast to HJbio-center, streptavidin addition to HJbio-end did not alter strand displacement by X-WRN and RPA. Approximately 95% of the A-oligo was displaced as ssDNA in the absence or presence of streptavidin (Figure 4A, lanes 2–4 or 7, respectively), and the three-way product observed in the HJbio-center reactions was not apparent. Furthermore, RPA alone does not melt the

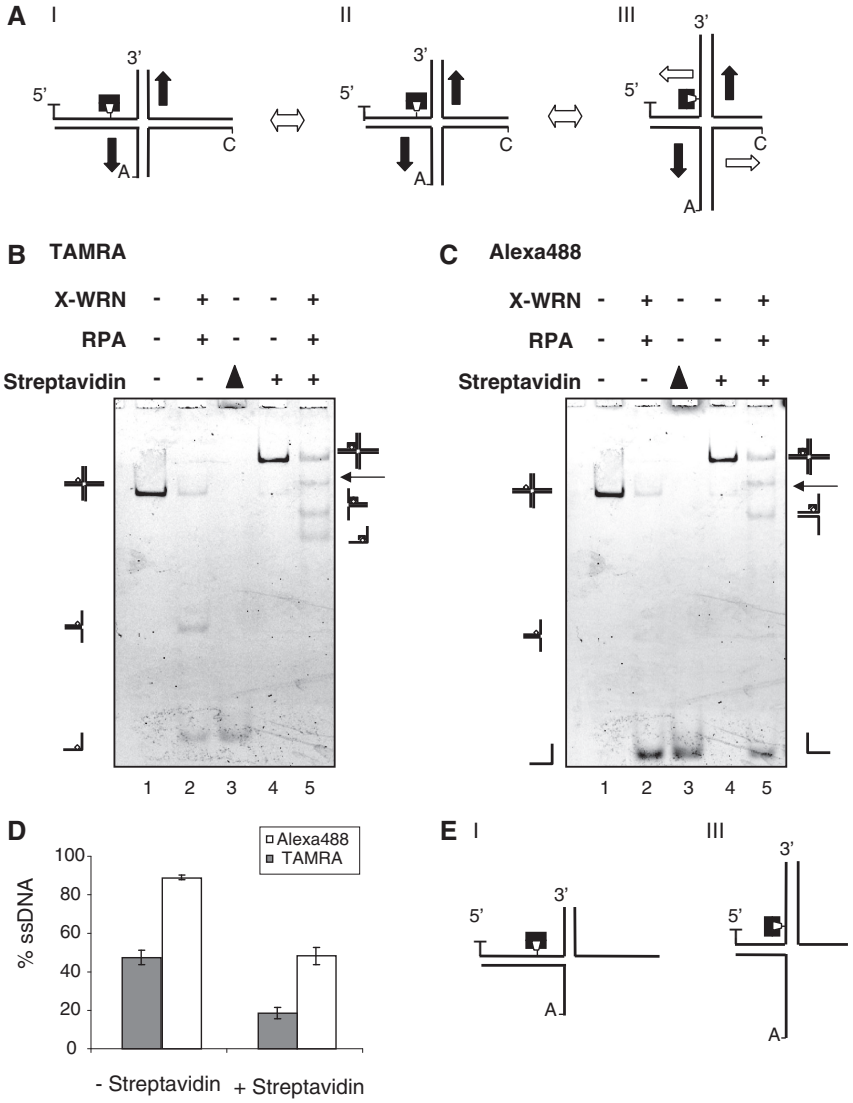

Figure 3. A biotin–streptavidin complex at the HJ core impedes WRN helicase activity. (**A**) The HJbio-center construct has a 12-nt homologous core that permits branch migration. The center construct (II) shows the HJ in a symmetric conformation with 25-bp arms. The left and right constructs (I and III) show the possible extreme conformations. T = TAMRA; C = Cy5; A = Alexa488; inverted trapezoid denotes a biotin moiety. Black box denotes a streptavidin. The predicated possible directions of unwinding are shown for each conformation; white arrow denotes unwinding along the horizontal axis; black arrow denotes unwinding along the vertical axis. (**B** and **C**) The HJbio-center substrate (0.5 nM) was pre-incubated without (lanes 1 and 2) or with (lanes 4 and 5) 30 nM streptavidin under standard reaction conditions prior the addition of 15 nM X-WRN and 45 nM RPA. The reactions were conducted for 1 h at 37°C. The products were run on an 8% native acrylamide gel for 2.5 h and visualized with a Typhoon Imager. Black triangle denotes boiled substrate lane. The TAMRA and Alexa488 emission channels are shown in (B) and (C), respectively. (**D**) Quantitation of ssDNA reaction products. The percent of T-oligo (gray bars) and A-oligo (white bars) detected as ssDNA product was quantitated as described in 'Materials and Methods' section. The values represent the mean and standard deviation from two to four independent experiments. (**E**) Schematic of the three-way product species that are generated upon addition of streptavidin.

HJ (Supplementary Figure S3). These data indicate that a biotin/streptavidin complex at the HJ core, but not at the HJ blunt end, inhibits WRN strand displacement.

TRF2 protects telomeric arm HJ DNA from WRN strand displacement activity

We hypothesized that TRF2 protects HJs from WRN activity since it stabilizes HR-like structures in the telomere from unwanted processing *in vivo* (7). To test this we examined the non-telomeric HJA, and designed an HJ containing three telomeric repeats in two duplex arms in a *trans* configuration (HJT; Table 1). A fully telomeric HJ construct would have been unstable due to spontaneous branch migration. TRF2 pre-binding to the substrate decreased the percent of WRN HJT strand displacement in a dose-dependent manner from 49% to 20% (Figure 5A and D). A TRF2-mediated decrease in exonuclease-degraded products was also observed (Alexa 488 channel, data not shown; TAMRA channel, Supplementary Figure S4). To determine whether TRF2 binding to the HJ core via its B-domain was responsible for WRN

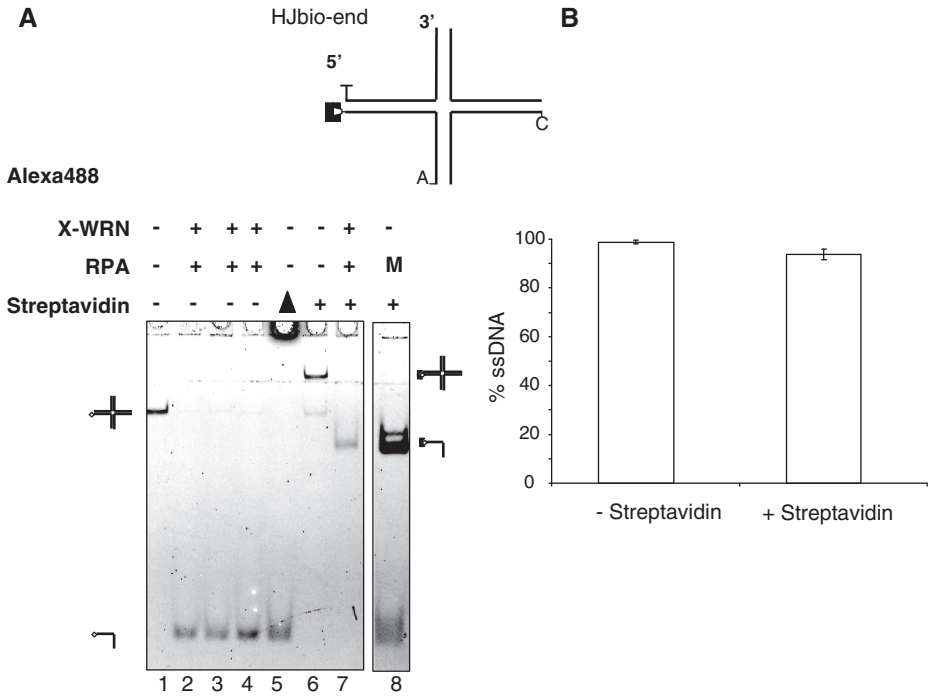

Figure 4. A biotin–streptavidin complex at the 3′-end of an HJ arm does not alter WRN helicase activity. The HJbio-end substrate has a biotin tag at the 3′-end of the A-oligo. T = TAMRA; C = Cy5; A = Alexa488; inverted trapezoid denotes a biotin moiety. Black box denotes streptavidin. (**A**) The HJbio-end (0.5 nM) substrate was pre-incubated without (lanes 2–4) or with (lanes 6 and 7) 30 nM streptavidin under standard reaction conditions prior the addition of 15 nM X-WRN and 45 nM RPA. The reactions were conducted for 1 h at 37°C. The products were run on an 8% native acrylamide gel for 2.5 h and visualized with a Typhoon Imager. Black triangle denotes boiled lane. M denotes an A-oligo ssDNA marker bound by streptavidin. The Alexa488 emission channel is shown. (**B**) Quantitation of ssDNA reaction products. The percent A-oligo detected as ssDNA product was quantitated as described in 'Materials and Methods' section. The values represent the mean and standard deviation from three independent experiments.

inhibition, we tested the non-telomeric HJA which lacks Myb binding sequences. In sharp contrast to the telomeric arm HJT, pre-binding TRF2 to HJA did not alter WRN unwinding (Figure 5B and D).

Next, we asked whether TRF2 interaction with the HJ arms via the Myb domain was responsible for TRF2 inhibition of WRN activity on the telomeric HJT. To test this, a TRF2 fragment with the N-terminal B domain deleted (TRF2ΔB) was used. The pre-incubation of telomeric HJT with TRF2ΔB exhibited no protective effect against WRN strand displacement activity (Figure 5C and D), nor did it alter the amount of exonuclease-degraded T-oligo (data not shown). These experiments indicate that TRF2 protects telomeric HJ DNA from WRN activity, but only on substrates containing binding sites for both the TRF2 B and Myb domains.

A previous study reported that TRF2 protects an HJ with two telomeric repeats in the center from cleavage by HJ resolvase enzymes (24). We tested the identical construct (HJM, Table 1) to determine whether TRF2 could provide a comparable protection from WRN strand displacement. While HJM has binding sites for both the TRF2 Myb and B domains, the Myb domain can only bind when the homologous core migrates to an extreme conformation with the two telomeric repeats in tandem on the same duplex arm (Figure 6A). In contrast to telomeric arm HJT, the pre-incubation of telomeric core HJM with increasing TRF2 concentrations did not alter the WRN strand displacement or exonuclease products (Figure 6B and D). To determine whether the lack of TRF2 inhibition resulted from WRN digestion into the Myb binding sequences, we repeated the experiment with the exonuclease-dead X-WRN. However, TRF2 did not alter X-WRN strand displacement of HJM either (Figure 6C and D).

RAP1 does not alter TRF2 protection of telomeric arm HJ from WRN activity

RAP1 is a member of the shelterin complex that binds TRF2, and is required along with TRF2 to protect telomeric ends from non-homologous end joining (NHEJ) (36,32). Therefore, we asked if RAP1 also cooperates with TRF2 to prevent telomeric HJ displacement. To test this, we pre-bound telomeric arm HJT with 25 nM TRF2 and increasing RAP1 concentrations (0–50 nM) prior to WRN addition (Figure 7B, lanes 2–5). While TRF2 inhibition of WRN was apparent, no significant difference in the amount of displaced HJ DNA was observed as a function of RAP1 concentration (Figure 7C). Nor did we detect any modulation of WRN activity by RAP1 (50 nM) alone (Figure 7B, lane 6).

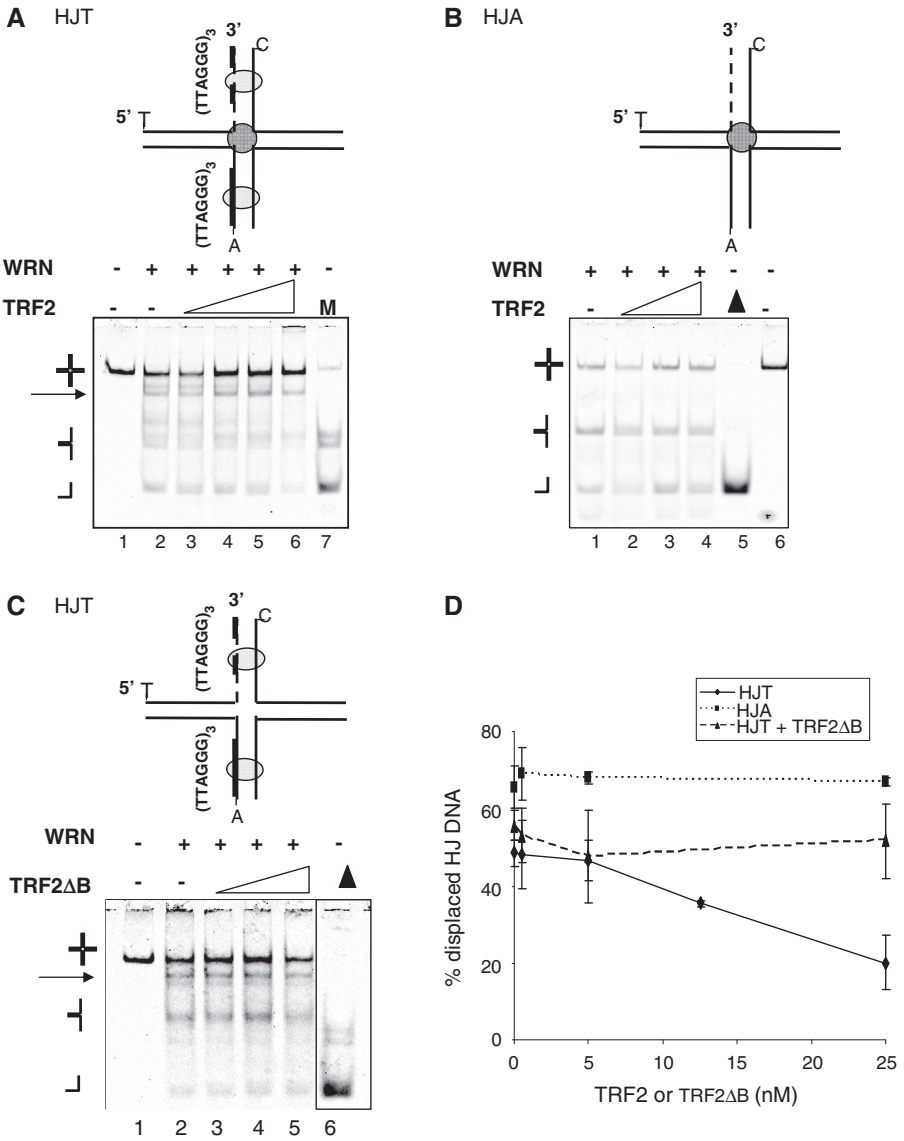

Figure 5. TRF2 inhibits WRN unwinding of HJ substrates with telomeric arms. A schematic of the telomeric arm (HJT) and non-telomeric HJA constructs are shown in (**A–C**). Thick black lines denote $(TTAGGG)_3$ repeats. T = TAMRA; C = Cy5; A = Alexa488. The 3′-end of the exonuclease-vulnerable T-oligo is highlighted as a dotted line. Predicted TRF2 binding sites are indicated with the circle (B-domain) and the ellipse (Myb domain). The substrates (0.5 nM) HJT (A) or HJA (B) were pre-incubated with 0, 0.5, 5, 12.5 or 25 nM TRF2 [(A), lanes 2–6, respectively] and 0, 0.5, 5 or 25 nM TRF2 [(B), lanes 1–4] in standard reaction buffer. The reactions were initiated by the addition of 19 nM WRN and reacted for 1 h at 37°C. The reactions were run on 8% native gels for 1.5 h and visualized with a Typhoon Imager. Scans of the Cy5 emission channel are shown in (A) and (B). Triangle indicates boiled substrate; M denotes a marker lane; arrows denote a triple-stranded species. (C) TRF2ΔB does not alter WRN unwinding of the telomeric HJ. The HJT (0.5 nM) substrate was pre-incubated with 0, 0.5, 5 or 25 nM TRF2ΔB (lanes 2–5) prior to the addition of 19 nM WRN. Reactions were for 1 h at 37°C, and were run on an 8% native gel. The scan from the Cy5 emission channel is shown. (**D**) Quantitation of HJ unwinding. The percent of C-oligo present in the HJ substrate was quantitated as a function of total C-oligo DNA in the reaction as described in 'Materials and Methods' section and plotted against TRF2 or TRF2ΔB concentration. The values represent the mean and standard deviation from at least three independent experiments.

TRF2 exhibits increased binding to telomeric HJ compared to non-telomeric HJ

We hypothesized that the mechanism by which TRF2 protects HJ DNA from WRN activity is via binding both the HJ core and the telomeric repeats in the HJ arms. Therefore, we predicted that TRF2 should exhibit increased binding to a telomeric HJ, compared to a non-telomeric HJ, since both TRF2 B and Myb domains can engage the telomeric HJ. We performed electrophoretic mobility shift assays to compare TRF2 binding to non-telomeric HJA and telomeric HJT and HJM. The migration of all three substrates was retarded by TRF2 in a protein concentration-dependent manner (Figure 8A, lanes 1–15). TRF2 shifted HJT to a higher migrating species compared to HJA or HJM, suggesting that more TRF2 molecules may be bound to the telomeric arm HJT substrate (Figure 8A, lanes 5, 10 and 15). A shifted HJ/TRF2 complex was apparent at 50 nM TRF2 for HJT and HJM, but was not detected until 125 nM

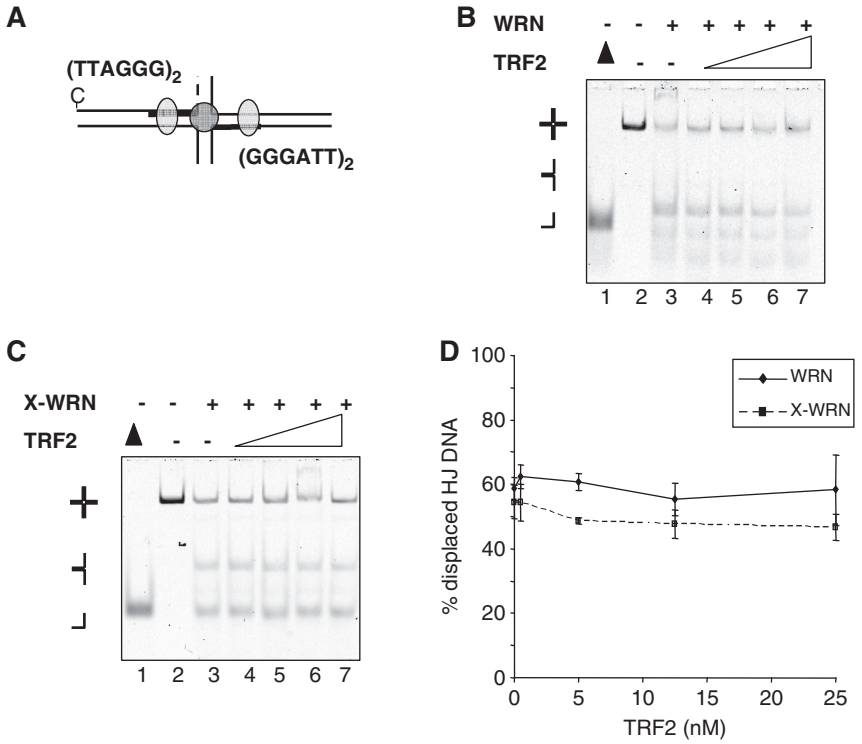

Figure 6. TRF2 fails to inhibit WRN helicase or exonuclease activities on an HJ with telomeric repeats confined to the core. (**A**) The HJM substrate has a 12-nt homologous core composed of two (TTAGGG)2 repeats, denoted by a thick black line. Shown is the conformation with a fully branch migrated core. The predicted TRF2 binding sites are indicated with the circle (B-domain) and the ellipse (Myb domain). C = Cy5 fluorophore. The 3′-end of the exonuclease vulnerable C-oligo is highlighted as a dotted line. (**B** and **C**) The HJM substrate (0.5 nM) was pre-incubated with either 0, 0.5, 5, 12.5 or 25 nM TRF2 (lanes 3–7) and reacted under standard conditions for 1 h with 25 nM WRN (B) or 40 nM X-WRN (C), respectively. The reactions were run on 8% native gels for 1.5 h and visualized with a Typhoon Imager. The scan from the Cy5 emission channel is shown. Triangle indicates boiled substrate. **(D)** Quantitation of HJ unwinding. The percent of C-oligo in the HJM displacement products were quantitated as a function of total C-oligo DNA as described in 'Materials and Methods' section and plotted against the TRF2 concentration. The values represent the mean and standard deviation from three separate experiments.

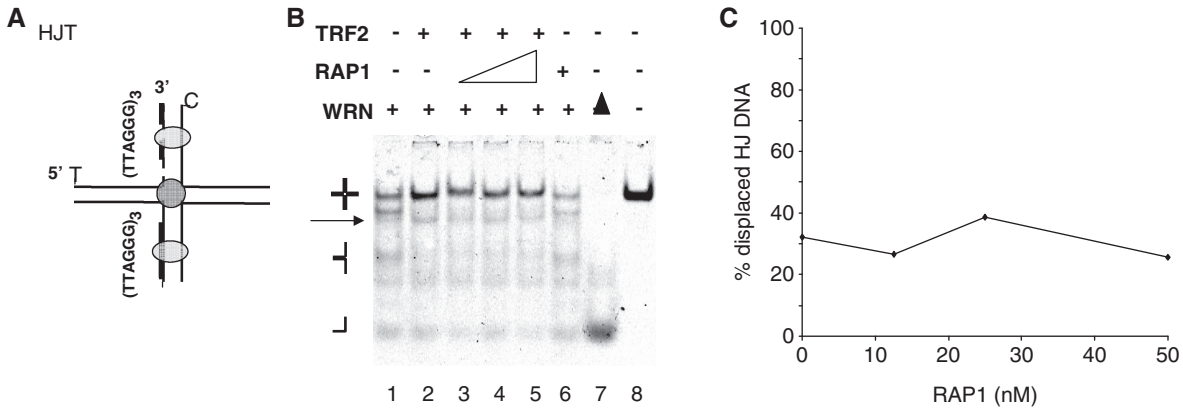

Figure 7. The RAP1/TRF2 complex inhibits WRN unwinding of HJ substrates with telomeric arms similar to TRF2 alone. (**A**) Schematic of the HJT construct is shown. Thick black lines denote $(TTAGGG)_3$ repeats. T = TAMRA; C = Cy5; A = Alexa488. The 3′-end of the exonuclease vulnerable T-oligo is highlight as a dotted line. Predicted TRF2 binding sites are indicated with the circle (B-domain) and the ellipse (Myb domain). (**B**) The substrate was pre-incubated with 25 nM TRF2 and 0, 12.5, 25 or 50 nM RAP1 (lanes 2–5) in standard reaction buffer. The reactions were initiated by the addition of 19 nM WRN (lanes 1–6) and reacted for 1 h at 37°C. Lane 6 contained 50 nM RAP1 and 19 nM WRN. The reactions were run on 8% native gels and visualized with a Typhoon Imager. Scans of the Cy5 emission channel are shown. Triangle indicates boiled substrate; arrows denote a triple-stranded species. (**C**) Quantitation of HJ unwinding. The percent of C-oligo present in the HJ products was quantitated as a function of total C-oligo DNA as described in 'Materials and Methods' section and plotted against RAP1 concentration.

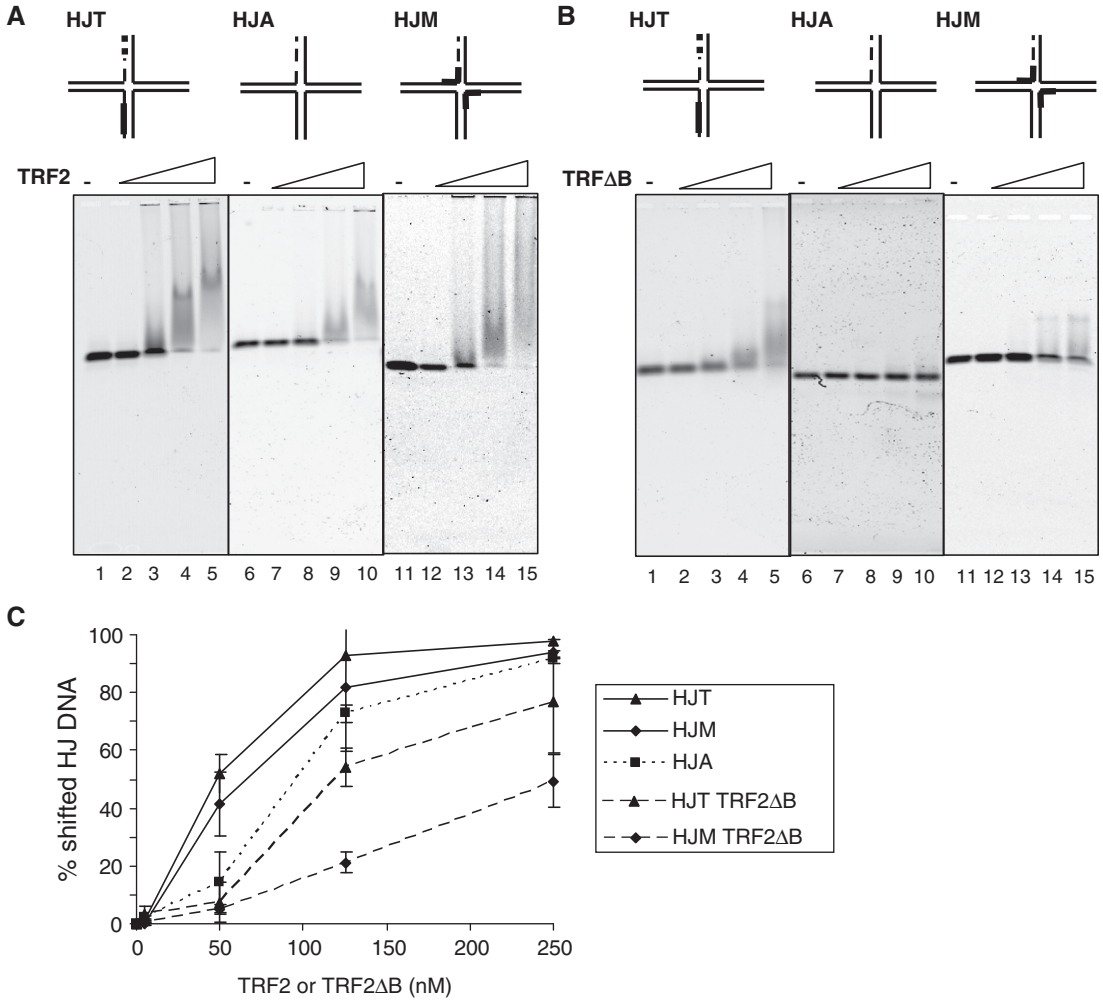

Figure 8. TRF2 and TRF2ΔB exhibit increased binding to telomeric HJ compared to non-telomeric HJ constructs. The substrates (5 nM) telomeric arm HJT (lanes 1–5), non-telomeric HJA (lanes 6–10), and telomeric core HJM (lanes 11–15) were reacted with either 0, 5, 50, 125 or 250 nM TRF2 (**A**) or TRF2ΔB (**B**), respectively, in standard reaction buffer supplemented with 5% glycerol for 20 min at 24°C. The reactions were loaded on a 1% 0.5× TBE agarose gel and electrophoresed for 1 h at 140 V in 4°C. Gels were scanned on a Typhoon Imager and visualized in the Cy5 channel. (**C**) Quantitation of the binding reactions. The percent of bound substrate was calculated as a function of total DNA in the Cy5 channel and plotted against TRF2 or TRF2ΔB concentration. Values represent the mean and standard deviation from two or three independent reactions.

TRF2 for HJA (Figure 8A, lanes 3, 8 and 13). The binding curves for the HJT and -M substrates showed a 50% shift by about 50 nM TRF2, compared to ~100 nM for HJA (Figure 8C).

Next, we tested whether the lack of TRF2ΔB inhibition of WRN on the HJT substrate resulted from a failure of the protein to bind the telomeric arms. The incubation of increasing TRF2ΔB concentrations with the non-telomeric HJA did not detectably alter substrate migration (Figure 7B, lanes 6–10), as expected, since this fragment lacks the B domain. In contrast, HJT migration was noticeably retarded at 125 and 250 nM TRF2ΔB concentrations (Figure 7B, lanes 4 and 5), with 54% and 74% of the HJT substrate shifted, respectively (Figure 7C). The TRF2 Myb domain can only bind a subset of HJM conformations (Figure 6A), thus, the percent of TRF2ΔB bound substrate was decreased compared to HJT (Figure 8C). In summary, these data indicate that TRF2 exhibits increased binding to telomeric versus non-telomeric HJs and shifts HJ DNA with telomeric arms (HJT) to higher migrating species compared to HJ DNA with a telomeric core (HJM).

DISCUSSION

The WRN helicase/exonuclease protein is a RecQ family helicase that displaces HJ DNA, consistent with a cellular function in restoring stalled replication forks and disrupting homologous recombination intermediates (1,2,4,6). Previous studies showed that TRF2 protects telomeric HJ DNA at the t-loop/D-loop from cleavage by endonucleases *in vivo* (16,25) and *in vitro* (24), but TRF2 protection from HJ displacement was not previously reported. Our results showed that TRF2 protects HJ DNA from WRN-mediated strand displacement, but only if TRF2 can simultaneously bind the HJ with both of its DNA-binding domains: (i) the B domain which

binds HJ DNA regardless of sequence and (ii) the Myb domain which binds telomeric duplex DNA (21,22). This is in contrast to previous research which showed that the B-domain is sufficient for protecting HJ DNA from enzymatic cleavage (24).

WRN mechanism of HJ strand displacement

The novel multiplex imaging of HJ strands in this study allowed us to elucidate mechanistic details of WRN strand displacement that would not be possible by labeling one strand of the construct as done previously. Our data are consistent with a mechanism by which WRN displaces HJs starting from the HJ center and processing outward. Specifically, on our substrate we propose WRN translocates 3′ to 5′ along the T-oligo from the center toward the 5′ TAMRA label at the blunt end (Figure 3). The first evidence was that a biotin–streptavidin barrier placed on the T-oligo at the HJ core led to a 2-fold reduction in single-stranded A- and T-oligo products (Figure 3). Second, the barrier at the HJ core also induced some trapping of the A- and T-oligos into novel two-way and three-way products that lacked the C-oligo (Figure 3) after WRN unwinding. This suggests that the biotin–streptavidin barrier inhibits WRN processivity along the A-T arm (Figure 3E, I) and the T-unlabeled arm (Figure 3E, III) depending on the barrier location in the specific mobile core conformation, but not along the C-oligo arms which never contains the barrier in any core conformation. Third, if WRN helicase initiated unwinding from an HJ arm blunt end and moved inward, then a barrier on the 3′-end of a strand should block WRN helicase. However, such a barrier had no effect on strand displacement, nor did it lead to novel 'trapped' products (Figure 4). In summary, although the WRN exonuclease can initiate at an HJ blunt end (Figure 1), the helicase does not, and thus, could not efficiently circumvent a protein bound to the HJ core such as TRF2.

Our results with the HJ barrier containing constructs corroborate electron micrographs showing WRN bound to the HJ center (28) and a protein–DNA cocrystal of RecG bound to a model replication fork (37). RecG and WRN belong to the SF2 superfamily of helicases (38), and RecG converts HJs into forked substrates and then into ssDNA similar to WRN (39,11) (Figure 1). The crystal structure shows a RecG monomer bound to the junction of a model replication fork (37), which resembles the junction of a regressed replication fork or HJ.

Mechanism of TRF2 inhibition of WRN telomeric arm HJ strand displacement

Our data help resolve a paradox of TRF2-WRN interactions. WRN is required for telomere preservation (8,40) and TRF2 stimulates WRN helicase on forked substrates (30), yet TRF2 prevents WRN promotion of aberrant telomere t-loop/D-loop HR cleavage (25). The WRN requirement for telomeric circle formation when the TRF2ΔB mutant is overexpressed (25) suggests TRF2 inhibits WRN-mediated branch migration at the telomere t-loop/D-loop. Here we report that TRF2 modulation of WRN activity is highly substrate dependent. At a 50:1 TRF2:HJ molar ratio, prebound TRF2 inhibited WRN strand displacement of an HJ with two telomeric arms by 50%, but unwinding of the non-telomeric HJ was unaffected (Figure 5). At this same ratio, nearly 100% of both the telomeric arm and non-telomeric HJs are bound by TRF2 (Figure 8), consistent with previous studies (21). This shows that TRF2 substrate binding via the B domain only (non-telomeric HJ) provides no protection against WRN activity (Figure 5). Consistent with this, the TRF2 Myb domain alone cannot protect the telomeric arm HJ (Figure 5C) or a telomeric fork (30) (the B-domain does not bind a fork), from WRN activity.

The mechanism of TRF2 protection against HJ cleavage differs from protection against WRN HJ strand displacement. A previous study showed that a 40:1 TRF2:HJ ratio reduced enzymatic HJ cleavage by 80% on an HJ with two telomeric repeats in the mobile center, and that protection was primarily via the B domain (24). With this same substrate (HJM, Figure 6A) even a 50:1 molar ratio of TRF2 to HJ provided no protection against WRN helicase activity (Figure 6B). One explanation for this difference is that while this HJ has binding sites for both the TRF2 B and Myb domains, both probably cannot bind at once. The footprint of a single Myb domain is YTAGGGTTR (41); thus, a TRF2 homodimer cannot bind this substrate with both Myb domains at once. A single Myb domain can bind only if the HJ mobile core has migrated to one extreme (Figure 6A), but it may not be sterically possible for the B domain to bind as well. Consistent with this, when the HJ-specific TRF2 B-domain was deleted the percent of TRF2 bound telomeric core HJM was half that of telomeric arm HJT (Figure 8C). Protection against WRN helicase activity requires both TRF2 domains to be bound, not just the B-domain as is the case with protection against cleavage. Poulet and colleagues (24) reported that the TRF2 B-domain 'melts' the mobile center of the HJ, creating an altered conformation that HJ cleaving enzymes cannot recognize. A melted HJ center would hardly discourage a helicase, particularly one that initiates displacement at the HJ center, such as WRN (Figures 3 and 4).

Several potential models might explain the TRF2 inhibition of WRN activity on telomeric arm HJ. In stark contrast to a biotin–streptavidin complex at the HJ core (Figure 3), a core bound TRF2 B-domain does not inhibit WRN (Figure 5), which rules out a TRF2 steric inhibition model. Since TRF2 interacts with WRN via the B-domain (25), we would have expected inhibition on a non-telomeric HJ, which was not the case (Figure 5B). Thus, TRF2 inhibition of WRN telomeric HJ activity is unlikely to be mediated by protein–protein interactions, which is the proposed mechanism for p53 inhibition of WRN HJ activity (42). Instead, we favor a model whereby both TRF2 DNA-binding domains must bind the HJ simultaneously in order to 'lock down' the substrate into a conformation that is unfavorable for WRN strand displacement or branch migration activity. While HJ constructs are often depicted as square-planar shapes,

crystallographic evidence indicates that duplex arms can stack on one other (43). Single-pair fluorescence resonance energy transfer (FRET) and structural studies showed that HJ DNA alternates between the stacked conformation and an open square-planar conformation, which is the form that branch migrates and is favored by proteins that promote HJ migration (37,44–46). Simultaneous interaction of TRF2 with the core and the telomeric arms might promote the stacked arm conformation, perhaps via TRF2 molecules bound to separate arms interacting with each other through dimerization or higher oligomeric forms. Consistent with this, the telomeric arm HJ (HJT) exhibited a slower TRF2-bound migrating species than either the non-telomeric (HJA) or telomeric core HJ (HJM) (Figure 8A), which likely reflects a larger oligomeric complex. Our results agree with previous studies that show TRF2 has higher affinity for HJs with telomeric repeats, compared to non-telomeric HJs (24). Therefore, the number of accessible telomeric binding sites is important for TRF2 HJ binding, and this correlates with protection from WRN activity. We suggest that a fully telomeric HJ would enjoy greater TRF2 protection since there are far more TRF2 binding sites compared to our hybrid constructs.

Role for RAP1/TRF2 complex in protection against HJ displacement

The current study extends our understanding of WRN function in the context of the mechanism of action of shelterin proteins at telomeres. While RAP1 forms a complex with TRF2 and is necessary to protect telomere ends from NHEJ (32), it does not alter TRF2-mediated inhibition of WRN on an HJ containing telomeric arms (Figure 7). RAP1 binds to the central TRF2 dimerization domain (36), whereas WRN interacts with the TRF2 N-terminal B domain (25). Thus, our biochemical data are consistent with cellular studies since RAP1 should still localize to telomeres with TRF2ΔB expression but offers no protection against aberrant HJ cleavage (25), and RAP1 does not localize to telomeres in the absence of TRF2 when protection against aberrant NHEJ is lost (47). Neither does RAP1 increase the binding affinity of TRF2 for telomeric DNA (48). Therefore, RAP1-mediated protection against NHEJ probably has no mechanistic basis in protection against WRN activity.

The yin and yang of WRN at telomeres

Telomeres are dynamic structures regulated by the interplay of multiple proteins composing both the shelterin complex and the numerous proteins that interact with shelterin. Many of these proteins become deleterious for telomere maintenance if dysregulated (7,49). WRN is necessary to prevent telomeric circle formation in telomerase-positive cells, but without full-length TRF2, WRN itself is required for telomere circle formation (25). In yeast, the TRF2 ortholog Taz1 similarly protects against telomere loss mediated by the WRN ortholog Rqh1 (50) in conjunction with the RPA ortholog Rad11 (51). Telomere preservation is restored in Taz1 mutants by either mutating a SUMOylation site on the Rgh1 protein (50) or by overexpressing the shelterin protein POT1 (51). By demonstrating that TRF2 can protect telomeric HJ DNA from WRN activity, our study provides a mechanistic basis for the cellular studies showing that TRF2 or Taz1 regulate WRN or Rqh1 activity, respectively.

In summary, we verified that WRN displaces HJs from the center and progresses outward, and that this strand displacement occurs simultaneously with WRN exonuclease activity. We found that TRF2 can protect telomeric HJs from WRN activity only if both TRF2 DNA-binding domains simultaneously engage the HJ core and the arms. Our biochemical studies provide an explanation for the cellular studies that indicate WRN adversely affects telomere processing in the absence of TRF2 (25). Understanding how shelterin accessory factors, such as WRN, are regulated by specific shelterin proteins is critical for defining mechanism of telomere loss and preservation, and the consequences of dysregulation for human disease.

SUPPLEMENTARY DATA

Supplementary Data are available at NAR Online.

ACKNOWLEDGEMENTS

We thank the members of the Opresko lab for their critical reading of the manuscript and feedback.

FUNDING

The National Institutes of Health (grant GM65484 to W.J.C.); Ellison Medical Foundation (to P.L.O.); National Institute of Environmental Health Sciences (grant number ES0515052 to P.L.O.); National Institute on Aging (grant number F30AG032861 to G.J.N.). Funding for open access charge: Ellison Medical Foundation (to P.L.O.); National Institute of Environmental Health Sciences (grant number ES0515052 to P.L.O.).

Conflict of interest statement. None declared.

REFERENCES

1. Kudlow,B.A., Kennedy,B.K. and Monnat,R.J. Jr (2007) Werner and Hutchinson-Gilford progeria syndromes: mechanistic basis of human progeroid diseases. *Nat. Rev. Mol. Cell Biol.*, **8**, 394–404.
2. Opresko,P.L. (2008) Telomere ResQue and preservation–roles for the Werner syndrome protein and other RecQ helicases. *Mech. Ageing Dev.*, **129**, 79–90.
3. Huang,S., Li,B., Gray,M.D., Oshima,J., Mian,I.S. and Campisi,J. (1998) The premature ageing syndrome protein, WRN, is a 3′–>5′ exonuclease. *Nat. Genet.*, **20**, 114–116.
4. Chu,W.K. and Hickson,I.D. (2009) RecQ helicases: multifunctional genome caretakers. *Nat. Rev. Cancer*, **9**, 644–654.
5. Sidorova,J.M., Li,N., Folch,A. and Monnat,R.J. Jr (2008) The RecQ helicase WRN is required for normal replication fork progression after DNA damage or replication fork arrest. *Cell Cycle*, **7**, 796–807.
6. Saintigny,Y., Makienko,K., Swanson,C., Emond,M.J. and Monnat,R.J. Jr (2002) Homologous recombination resolution defect in Werner syndrome. *Mol. Cell Biol.*, **22**, 6971–6978.

7. Palm,W. and de Lange,T. (2008) How shelterin protects mammalian telomeres. *Annu. Rev. Genet.*, **42**, 301–334.
8. Crabbe,L., Verdun,R.E., Haggblom,C.I. and Karlseder,J. (2004) Defective telomere lagging strand synthesis in cells lacking WRN helicase activity. *Science*, **306**, 1951–1953.
9. Wyllie,F.S., Jones,C.J., Skinner,J.W., Haughton,M.F., Wallis,C., Wynford-Thomas,D., Faragher,R.G. and Kipling,D. (2000) Telomerase prevents the accelerated cell ageing of Werner syndrome fibroblasts. *Nat. Genet.*, **24**, 16–17.
10. Crabbe,L., Jauch,A., Naeger,C.M., Holtgreve-Grez,H. and Karlseder,J. (2007) Telomere dysfunction as a cause of genomic instability in Werner syndrome. *Proc. Natl Acad. Sci. USA*, **104**, 2205–2210.
11. Mohaghegh,P., Karow,J.K., Brosh,J.R. Jr, Bohr,V.A. and Hickson,I.D. (2001) The Bloom's and Werner's syndrome proteins are DNA structure-specific helicases. *Nucleic Acids Res.*, **29**, 2843–2849.
12. Opresko,P.L., Sowd,G. and Wang,H. (2009) The Werner syndrome helicase/exonuclease processes mobile D-loops through branch migration and degradation. *PLoS One*, **4**, e4825.
13. Constantinou,A., Tarsounas,M., Karow,J.K., Brosh,R.M., Bohr,V.A., Hickson,I.D. and West,S.C. (2000) Werner's syndrome protein (WRN) migrates Holliday junctions and co-localizes with RPA upon replication arrest. *EMBO Rep.*, **1**, 80–84.
14. Makarov,V.L., Hirose,Y. and Langmore,J.P. (1997) Long G tails at both ends of human chromosomes suggest a C strand degradation mechanism for telomere shortening. *Cell*, **88**, 657–666.
15. Stansel,R.M., de Lange,T. and Griffith,J.D. (2001) T-loop assembly in vitro involves binding of TRF2 near the 3′ telomeric overhang. *EMBO J.*, **20**, 5532–5540.
16. Wang,R.C., Smogorzewska,A. and de Lange,T. (2004) Homologous recombination generates T-loop-sized deletions at human telomeres. *Cell*, **119**, 355–368.
17. Verdun,R.E. and Karlseder,J. (2006) The DNA damage machinery and homologous recombination pathway act consecutively to protect human telomeres. *Cell*, **127**, 709–720.
18. Karlseder,J., Hoke,K., Mirzoeva,O.K., Bakkenist,C., Kastan,M.B., Petrini,J.H. and de Lange,T. (2004) The telomeric protein TRF2 binds the ATM kinase and can inhibit the ATM-dependent DNA damage response. *PLoS Biol.*, **2**, E240.
19. Amiard,S., Doudeau,M., Pinte,S., Poulet,A., Lenain,C., Faivre-Moskalenko,C., Angelov,D., Hug,N., Vindigni,A., Bouvet,P. *et al.* (2007) A topological mechanism for TRF2-enhanced strand invasion. *Nat. Struct. Mol. Biol.*, **14**, 147–154.
20. Denchi,E.L. and de Lange,T. (2007) Protection of telomeres through independent control of ATM and ATR by TRF2 and POT1. *Nature.*, **448**, 1068–1071.
21. Fouche,N., Cesare,A.J., Willcox,S., Ozgur,S., Compton,S.A. and Griffith,J.D. (2006) The basic domain of TRF2 directs binding to DNA junctions irrespective of the presence of TTAGGG repeats. *J. Biol. Chem.*, **281**, 37486–37495.
22. Hanaoka,S., Nagadoi,A. and Nishimura,Y. (2005) Comparison between TRF2 and TRF1 of their telomeric DNA-bound structures and DNA-binding activities. *Protein Sci.*, **14**, 119–130.
23. Cesare,A.J. and Griffith,J.D. (2004) Telomeric DNA in ALT cells is characterized by free telomeric circles and heterogeneous t-loops. *Mol. Cell Biol.*, **24**, 9948–9957.
24. Poulet,A., Buisson,R., Faivre-Moskalenko,C., Koelblen,M., Amiard,S., Montel,F., Cuesta-Lopez,S., Bornet,O., Guerlesquin,F., Godet,T. *et al.* (2009) TRF2 promotes, remodels and protects telomeric Holliday junctions. *EMBO J.*, **28**, 641–651.
25. Li,B., Jog,S.P., Reddy,S. and Comai,L. (2008) WRN controls formation of extrachromosomal telomeric circles and is required for TRF2DeltaB-mediated telomere shortening. *Mol. Cell Biol.*, **28**, 1892–1904.
26. Fouche,N., Ozgur,S., Roy,D. and Griffith,J.D. (2006) Replication fork regression in repetitive DNAs. *Nucleic Acids Res.*, **34**, 6044–6050.
27. Shen,J.C. and Loeb,L.A. (2000) Werner syndrome exonuclease catalyzes structure-dependent degradation of DNA. *Nucleic Acids Res.*, **28**, 3260–3268.
28. Compton,S.A., Tolun,G., Kamath-Loeb,A.S., Loeb,L.A. and Griffith,J.D. (2008) The Werner syndrome protein binds replication fork and Holliday junction DNAs as an oligomer. *J. Biol. Chem.*, **283**, 24478–24483.
29. Machwe,A., Xiao,L. and Orren,D.K. (2004) TRF2 recruits the Werner syndrome (WRN) exonuclease for processing of telomeric DNA. *Oncogene*, **23**, 149–156.
30. Opresko,P.L., von Kobbe,C., Laine,J.P., Harrigan,J., Hickson,I.D. and Bohr,V.A. (2002) Telomere-binding protein TRF2 binds to and stimulates the Werner and Bloom syndrome helicases. *J. Biol. Chem.*, **277**, 41110–41119.
31. Sowd,G., Lei,M. and Opresko,P.L. (2008) Mechanism and substrate specificity of telomeric protein POT1 stimulation of the Werner syndrome helicase. *Nucleic Acids Res.*, **36**, 4242–4256.
32. Bae,N.S. and Baumann,P. (2007) A RAP1/TRF2 complex inhibits nonhomologous end-joining at human telomeric DNA ends. *Mol. Cell*, **26**, 323–334.
33. Zhitkovich,A. and Costa,M. (1992) A simple, sensitive assay to detect DNA-protein crosslinks in intact cells and in vivo. *Carcinogenesis*, **13**, 1485–1489.
34. Opresko,P.L., Laine,J.P., Brosh,R.M. Jr, Seidman,M.M. and Bohr,V.A. (2001) Coordinate action of the helicase and 3′ to 5′ exonuclease of Werner syndrome protein. *J. Biol. Chem.*, **276**, 44677–44687.
35. Machwe,A., Xiao,L., Groden,J. and Orren,D.K. (2006) The Werner and Bloom syndrome proteins catalyze regression of a model replication fork. *Biochemistry*, **45**, 13939–13946.
36. Li,B., Oestreich,S. and de Lange,T. (2000) Identification of human Rap1: implications for telomere evolution. *Cell*, **101**, 471–483.
37. Singleton,M.R., Scaife,S. and Wigley,D.B. (2001) Structural analysis of DNA replication fork reversal by RecG. *Cell*, **107**, 79–89.
38. Pyle,A.M. (2008) Translocation and unwinding mechanisms of RNA and DNA helicases. *Annu. Rev. Biophys.*, **37**, 317–336.
39. Lloyd,R.G. and Sharples,G.J. (1993) Processing of recombination intermediates by the RecG and RuvAB proteins of Escherichia coli. *Nucleic Acids Res.*, **21**, 1719–1725.
40. Laud,P.R., Multani,A.S., Bailey,S.M., Wu,L., Ma,J., Kingsley,C., Lebel,M., Pathak,S., DePinho,R.A. and Chang,S. (2005) Elevated telomere-telomere recombination in WRN-deficient, telomere dysfunctional cells promotes escape from senescence and engagement of the ALT pathway. *Genes Dev.*, **19**, 2560–2570.
41. Fairall,L., Chapman,L., Moss,H., de Lange,T. and Rhodes,D. (2001) Structure of the TRFH dimerization domain of the human telomeric proteins TRF1 and TRF2. *Mol. Cell*, **8**, 351–361.
42. Yang,Q., Zhang,R., Wang,X.W., Spillare,E.A., Linke,S.P., Subramanian,D., Griffith,J.D., Li,J.L., Hickson,I.D., Shen,J.C. *et al.* (2002) The processing of Holliday junctions by BLM and WRN helicases is regulated by p53. *J. Biol. Chem.*, **277**, 31980–31987.
43. Khuu,P.A., Voth,A.R., Hays,F.A. and Ho,P.S. (2006) The stacked-X DNA Holliday junction and protein recognition. *J. Mol. Recognit.*, **19**, 234–242.
44. Karymov,M., Daniel,D., Sankey,O.F. and Lyubchenko,Y.L. (2005) Holliday junction dynamics and branch migration: single-molecule analysis. *Proc. Natl Acad. Sci. USA*, **102**, 8186–8191.
45. McKinney,S.A., Freeman,A.D., Lilley,D.M. and Ha,T. (2005) Observing spontaneous branch migration of Holliday junctions one step at a time. *Proc. Natl Acad. Sci. USA*, **102**, 5715–5720.
46. Parsons,C.A., Stasiak,A., Bennett,R.J. and West,S.C. (1995) Structure of a multisubunit complex that promotes DNA branch migration. *Nature*, **374**, 375–378.

47. Sarthy,J., Bae,N.S., Scrafford,J. and Baumann,P. (2009) Human RAP1 inhibits non-homologous end joining at telomeres. *EMBO J.*, **28**, 3390–3399.
48. Li,B., Oestreich,S. and de Lange,T. (2000) Identification of human Rap1: implications for telomere evolution. *Cell*, **101**, 471–483.
49. de Lange,T. (2009) How telomeres solve the end-protection problem. *Science*, **326**, 948–952.
50. Rog,O., Miller,K.M., Ferreira,M.G. and Cooper,J.P. (2009) Sumoylation of RecQ helicase controls the fate of dysfunctional telomeres. *Mol. Cell*, **33**, 559–569.
51. Kibe,T., Ono,Y., Sato,K. and Ueno,M. (2007) Fission yeast Taz1 and RPA are synergistically required to prevent rapid telomere loss. *Mol. Biol. Cell*, **18**, 2378–2387.